Rijksuniversiteit Groningen - Review Paper for the Top Master in Nanoscience

Enhancing the Spin-Coherence Times for Nanodiamonds with Near-Surface NV-centres for Free Radical Detection

Author: *Virun D. Malalasena - S4716280*

Supervisor: *Prof. Dr. Ir. Caspar van der Wal*

April 13, 2025

Abstract

In the medical field, magnetic resonance imaging systems generally lack the sensitivity to detect weak signals associated with free radicals, such as those arising from their magnetic moments. This is important as conditions such as sepsis are associated with the presence of free radicals in patients. Quantum sensors are promising devices that offer better resolution and sensitivity compared to their classical counterparts, as they take advantage of effects such as spin dynamics. Nitrogen-vacancy centres (NV-centres), a type of quantum sensor, are situated near the nanodiamond surface and can detect free radicals through T_1 relaxometry. Beyond their relaxation times, the spin-coherence time of the NV-centres can serve as an additional parameter that enables more precise studies of free radicals. However, surface characteristics, namely paramagnetic defects and dangling bonds, significantly reduce the coherence time of the NV-centre. This review paper explores various synthesis techniques and surface treatments to improve the surface characteristics of the nanodiamonds. Additionally, the coherence time of the NV centre is determined through microwave pulsed optically detected magnetic resonance experiments and can be extended using specific pulse sequences. This paper will also examine the coherence times achieved with various microwave pulse sequences.

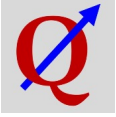

Contents

1 Introduction

Developments within the medical field often benefit from instruments with improved sensitivity and resolution, which allows for detecting weaker signals and resolving finer-scale details [1], [2]. Examples include the development of fluorescence-guided surgery [3], which allows surgeons to conduct intraoperative imaging and define tumour boundaries better [4]. This method not only enhances tumour resection but minimizes tumour recurrence [5]. Another device category is the quantum sensor [1]. These sensors use quantum mechanical effects such as quantum coherence and spin dynamics, which are not measurable with classically-based sensors [6].

Quantum sensors include colour centres, such as nitrogen-vacancy centres (NV-centres), which are point defects situated near the surface of nanodiamonds (NDs), where a nitrogen atom replaces a carbon atom after an adjacent carbon vacancy (Figure 1(a)) [7]. NV-centres may occur naturally, but studies use synthetic NDs to allow more control over their properties [7]. These defects influence the optical properties by giving NDs fluorescent emission capabilities. The use of NDs in healthcare has increased due to their biocompatibility [8], cost-effectiveness [8], and their production and size enable the study of a cell's intracellular movement [9]. Additionally, NDs with NV-centres are most widely employed for diamond magnetometry [10].

Diamond magnetometry is a technique that may use NV-centres in NDs to monitor changes in the NV-centres spin state when in a magnetic environment. This allows for detecting weak magnetic fields to a scale that conventional magnetic resonance imaging systems generally struggle with [11]. For example, this has allowed researchers to detect magnetic moments that may be linked with free radicals in biological cells [12]. This is remarkably valuable as the presence of free radicals is associated with conditions such as sepsis, which is responsible for 11 million annual deaths [13].

When studying samples that may contain free radicals, the observed fluorescence intensity from NV-centres is lower compared to samples without free radicals [9]. The fluorescent intensity is related to T_1 relaxometry, which measures the longitudinal relaxation time taken for the NV-centres spin system to return to thermal equilibrium after being optically disturbed [14], specifically, through the use of a 532 nm green laser [15]. Free radicals may have an associated magnetic moment [16], which affects the exchange of energy between the NV-centre and its surroundings [7]. This causes the relaxation time to decay more rapidly, resulting in a reduction of fluorescence intensity.

NV-centres are rich in spin dynamics and offer more than their spin-relaxation characteristic [17]. This review paper aims to investigate different experimental techniques which enhance the coherence time of the NV-centres, enabling it to be an additional parameter used to study free radicals with higher sensitivity. However, surface characteristics such as paramagnetic defects [18] and dangling bonds [19] reduce coherence times. Literature reports measured coherence times of the NV-centres being two orders of magnitude lower than their relaxation times [20]. Therefore, different synthesis techniques and surface treatments will be investigated to reduce surface defects. In addition, the coherence time is measured through microwave pulsed optically detected magnetic resonance (ODMR) experiments [15] and is influenced by the pulse sequence used. Thus, various pulse sequences and their respective coherence time will be explored.

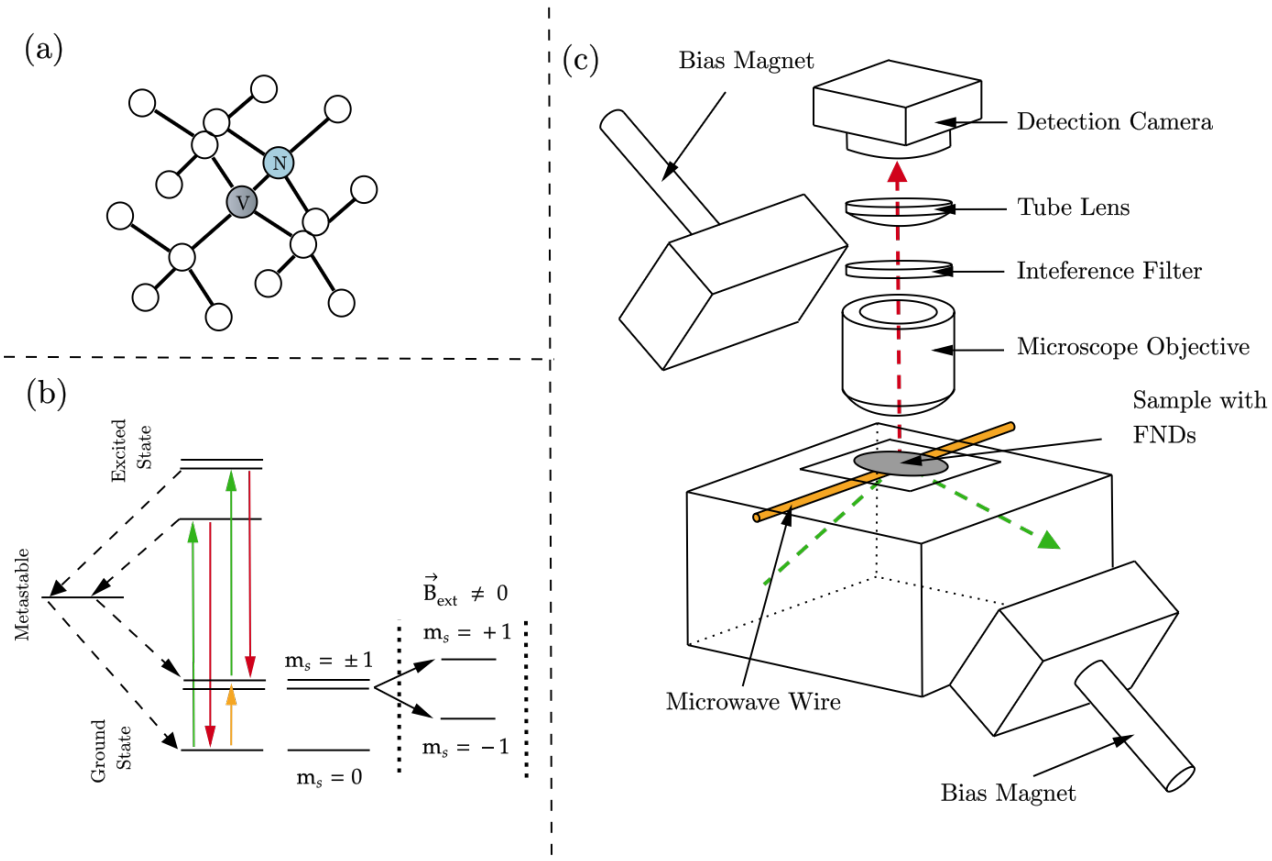

Figure 1: *(a) Diamond lattice with an NV centre where N represents a nitrogen atom, and V represents a vacancy (Figure inspired by [21]). (b) Jablonski diagram of the NV-centre, where the green arrows represent excitations and the red arrows represent relaxation through fluorescence. The orange arrow represents the spin-flip transition after applying a specific microwave frequency. Additionally, the Zeeman effect causes $m_s = \pm 1$ states to split in the presence of an external magnetic field (Figure inspired by [10]). (c) Experimental setup for exciting samples containing NDs. After applying a green laser and microwave pulses, the corresponding optically detected magnetic resonance spectra and fluorescence emission are recorded (Figure inspired by [1]).*

2 Magnetic Reasonance Imaging

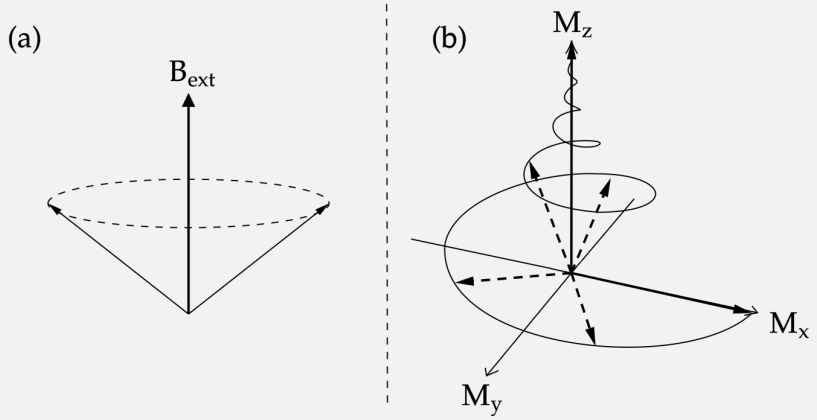

Figure 2: *(a) Larmor precession of the hydrogen nuclear spin when subjected to an external magnetic field. (b) Changes transverse (M_x and M_y plane) and longitudinal (M_z plane) magnetization during a $\frac{\pi}{2}$ radio-frequency pulse (Figure inspired by the GitHub animation by Steren Giannini [a]).*

The following grey box was written based on the content from [22], [14], [23], [24], and Questions and Answers in MRI[b] by Allen D. Elster, MD. Magnetic Resonance Imaging (MRI) machines in clinics and hospitals offer a non-invasive and non-ionizing method for imaging a patient's spinal cord to their kidneys. In these machines, the patient lies down on a platform that is slid into the MRI machine, which contains superconducting magnets that generate a magnetic field (B_{ext}) along the patient's body (the longitudinal axis). The interaction between the hydrogen nuclear spins and B_{ext} causes a Zeeman effect, which lifts the energy degeneracy, splitting it into two non-degenerate energy levels. Hydrogen nuclear spins in the spin-up state have associated magnetic moments which precess parallel to B_{ext}. Whereas hydrogen nuclear spins in the spin-down state have associated magnetic moments which precess antiparallel to B_{ext}. The precession frequency of the hydrogen nuclear spins in either the spin-up or spin-down state can be expressed through the Larmor equation:

$$\omega_0 = \gamma B_{ext}. \tag{1}$$

ω_0 is the angular frequency at which the spins precess, and γ is known as the gyromagnetic ratio for hydrogen nuclear spin (Figure 2(a)). In addition, the population distribution of spin-up and spin-down hydrogen nuclei can be expressed through the Boltzmann Distribution:

$$\frac{N_+}{N_-} = e^{\frac{-\Delta E}{kT}}. \tag{2}$$

N_- represents the population of hydrogen nuclear spins in the spin-up state, which slightly outnumbers N_+, which is the population of hydrogen nuclear spins in the spin-down state. The energy difference between energy levels associated with spin populations N_- and N_+ is expressed by ΔE. Here, the energy associated with spin population N_- is lower in comparison to that of spin population N_+. In addition, k represents the Boltzmann constant, and T is the temperature. As there is a population difference between N_- and N_+ (equation 2), this results in results in a net magnetization vector (M_0) which aligns parallel to B_{ext}.

To produce an image, a $\frac{\pi}{2}$ radio-frequency (RF) excitation pulse is transmitted via RF coils in the MRI machine, which tips M_0 to point in the transverse plane. Over time, M_0 will spiral and gradually realigns with B_{ext} (Figure 2(b)). The time taken for 63% of the longitudinal magnetization, the component of the magnetization vector in the longitudinal plane (Figure 2(b)), to return to its equilibrium state is known as the T_1 relaxation time. Whereas the time taken for 63% of the transverse magnetization, the component of the magnetization vector in the transverse plane (Figure 2(b)), to decay to zero is known as the T_2 coherence time. As this happens, hydrogen nuclear spins emit RF signals, which are received by RF coils within the MRI machine. As the local environment within a patient varies, how the longitudinal and transverse magnetization evolves will also be different. This gives rise to signal contrast between the various body parts of the patient, thus each body part, tissues, and organ of the patient have its own respective T_1 relaxation time and T_2 coherence

times. Analysing the emitted RF signals from hydrogen nuclear spins, one can generate an image, where the contrast between different regions can be investigated due to differing T_1 relaxation time and T_2 coherence time.

Figure 3: *MRI image of a fetus at 26 weeks gestation. The face of the fetus is indicated via the white arrow. Figure adapted from Amin et al. [25].*

However, this is not the complete story. The emitted RF signal by hydrogen nuclear spins occurs via free induction decay (FID), where the signal decays exponentially over time. This rapid decay is a result of not only spin-spin interaction but also due to inhomogeneous magnetic fields. This causes the hydrogen nuclear spins to precess at different angular frequencies, causing them to dephase in the transverse plane, leading to a faster decay in transverse magnetization. The decay due to a combination of both spin-spin interactions and magnetic field inhomogeneities is referred to as T_2^* dephasing effects. To combat T_2^* dephasing effects, by introducing different RF-pulse sequences, the spins can have their phase coherence re-established. Examples include the Hahn-Echo sequence (Figure 8(a)), which can cancel out effects due to magnetic field inhomogeneities, which extend the spin-coherence times. This significantly reduces the signal decay, thus allowing for an image to be generated with diagnostic relevance (Figure 3).

[a] https://github.com/steren/mri-spin
[b] https://mriquestions.com/index.html

3 NV-Centre Basics

As previously discussed, NV-centres are point defects situated near the surface of NDs, where a nitrogen atom replaces a carbon atom next to an adjacent carbon vacancy (Figure 1(a)) [7]. NV-centres exist in three different charge states, namely the NV^0, NV^+, and NV^- states. Between these three different charge states, the NV^- will be studied as it is the only charged state that is both paramagnetic and optically active [15].

When considering the NV^- charge state[1], it has a trapped electron with three unpaired electrons due to three nearby carbon atoms, along with an unpaired electron pair from nitrogen [7]. This forms a six-electron configuration, which can be thought of as two holes in a completely occupied n = 2 atomic shell. This gives rise to singlet and triplet states, where its energy level consists of a ground triplet state, an excited triplet state, and a metastable state (Figure 1(b)) [7], [26]. At $B_{ext} = 0$, the ground triplet state consists of two sublevels, namely $m_s = 0$ and the $m_s = \pm 1$, where an energy difference of 2.9 GHz [15]. Likewise, the excited triplet state consists of $m_s = 0$ and $m_s = \pm 1$ sublevels, however, with an energy difference of 1.4 GHz [15].

For optical transitions, a green laser of 532 nm may be used, where excitation via the NV-centres consists of a zero-phonon line at 637 nm [7], [15]. This corresponds to a direct transition from the excited triplet state back to the ground triplet state, resulting in a radiative red fluorescence emission seen in the diamonds after excitation [26]. A few percent of photons are emitted via the zero-phonon line, whereas the presence of phonon sidebands accounts for most of the NV-centres luminescence (between ranges of 630-800 nm) [15]. The fluorescence intensity is dependent on the NV-centre's spin state, where an excitation from the $m_s = 0$ state would result in more emitted fluorescence in comparison to if the NV-centre were to be excited from the $m_s = \pm 1$ state [26]. This is because the NV-centre undergoes an inter-system crossing through the metastable state, which causes a decrease in the observed fluorescence intensity [26]. Moreover, microwave frequencies of 2.9 GHz can be used to excite the NV-centre from the $m_s = 0$ sublevel to the $m_s = \pm 1$ [15], [26]. This process is achieved using ODMR experiments by conducting a microwave sweep (which is supplied via a wire - Figure 1(c)) [26]. Overall, this is an important quality as it allows various physical quantities that influence the NV-centre to be detected [26].

The spin-dependent optical properties of the NV-centre allow for useful nanoscale sensing applications, where its relaxation is primarily studied. Namely, relaxation time is defined as the rate of transition between the $m_s = 0$ to $m_s = \pm 1$ spins sublevels in the ground state [15]. Experimentally, setups as those seen in Figure 1(c) involve applying a green laser pulse which initializes the NV-centre into the $m_s = 0$ state (otherwise known as its bright state) [9]. The laser is then turned off for some time, otherwise known as its dark time [9], [15]. In this period, NV-centre spin state returns to its thermal equilibrium state, followed by a readout laser pulse [9] which measures the fluorescence via a detection camera (Figure 1(c)). When the dark time increases, the fluorescence intensity will decrease as it is dependent on the spin state [9]. The relaxation time can be determined using the following equation:

$$I_f \propto e^{\frac{-t}{T_1}}. \tag{3}$$

Where I_f represents the fluorescence intensity, and t is the dark time. Using this relation, the relaxation time can be determined. To determine the coherence time of the NV-centre, microwave pulsed ODMR may be applied before and after the initial and readout laser pulses [15]. Different sequences may be applied, such as the Ramsey sequence, which follows an initial and readout $\frac{\pi}{2}$ microwave pulse, where the time

[1] From this point on, whenever an NV-centre is brought up, it will be in context to the NV^- charge state.

between the pulse is its free evolution time [15], [17]. Typically, this sequence is repeated multiple times, which results in oscillations (Ramsay fringes) [15]. In the case of the Ramsey sequence, by analysing how the Ramsey fringes decay with time, one can obtain the T_2^* dephasing time.

To detect magnetic fields, the condition $B_{ext} \neq 0$ causes a Zeeman splitting, which causes the lifting of the degeneracy between $m_s = +1$ and $m_s = -1$ [26]. This can be seen in the ODMR spectrum, wherein the presence of an external magnetic field, a double minimum, where the distance between the minima corresponds to the strength of B_{ext} [15], [26]. This splitting plays an important role in understanding the impact that environmental magnetic noise has on the relaxation and coherence times. For relaxation times, environmental fluctuations may accelerate spin relaxation, causing shorter relaxation times. When looking at the coherence times, magnetic noise may disrupt the phase evolution of the NV-centre's spin state, leading to shorter coherence times.. This method is particularly useful as it allows for the detection of magnetic species, such as free radicals.

4 Optimising the Surface Characteristics of NDs

Scientists often perceive diamonds for their chemically inert properties, sparking interest in their use for biomedical applications, for example, their presence in coatings for artificial heart valves, which increases implant lifetime [27]. However, in the context of NDs, the surface of synthetically synthesised NDs may have paramagnetic defects [18] and dangling bonds [19], particularly detrimental to quantum sensing, and may compromise their biocompatibility. Kim *et al.* report that both magnetic and electric noise influence spin decoherence [28], which results in shorter coherence times. Thus, this review paper will explore different synthesis techniques and various surface treatments to reduce the presence of paramagnetic defects and dangling bonds.

4.1 Removing Paramagnetic Defects

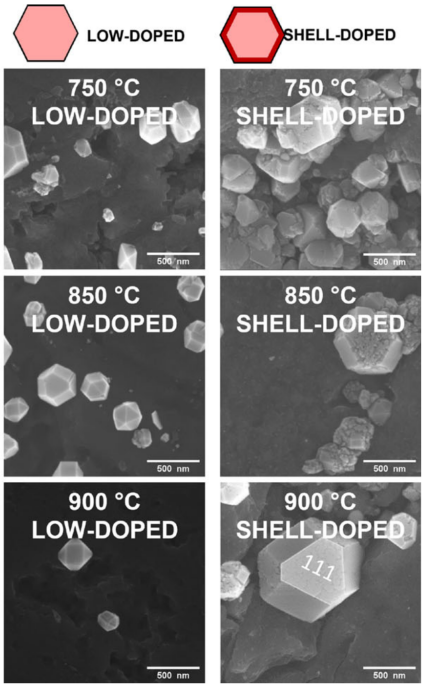

Figure 4: *The structural evolution of NDs for both low-doped and shell-doped NDs as the temperature is increased. In addition, due to a high nitrogen concentration, shell-doped particles exhibited preferential re-nucleation on their {111} facets. Figure adapted from Prooth et al. [29].*

The creation of NDs started in the USSR during the 1960s and was made through detonation techniques [8]. This process involved graphite precursors, which are subjected to a controlled explosion, where the shock wave pressure and temperature cause a phase transition to a diamond structure [8], [30]. NDs synthesised in this manner are known to be very cost-effective and biocompatible [8]. However, these NDs not only strongly aggregate but also exhibit a noticeable concentration of both paramagnetic defects and dangling bonds [31]. Making detonation a less favoured synthesis technique in terms of better surface quality.

High-pressure, high-temperature annealing (HPHT) is another technique commonly used to synthesise NDs, as the name suggests, involves the use of annealing diamonds at high temperature and high-pressure conditions [32], [33]. These diamonds can later be broken down into NDs via physical or chemical methods. Unfortunately, this method is known for giving rise to many paramagnetic defects [34].

Another method for growing NDs is chemical vapour deposition (CVD), which is shown to reduce paramagnetic effects significantly [34]. This method is primarily used for growing bulk diamonds. However, in 2023, Prooth *et al.* were able to synthesise NDs of roughly 60 nm [29]. This paper discusses a bottom-up approach, involving the use of carbon precursors to grow NDs via CVD between temperatures of 750°C and 900°C. Two sets of NDs were synthesised, NDs with low nitrogen doping and NDs with shell-doped nitrogen layer (Figure 4). Prooth *et al.* were able to show a significant increase in relaxation times using CVD in comparison to HPHT methods, however, the coherence time of the NDs did not show such improvement [29]. This discrepancy is reported to be due to the formation of substitutional nitrogen (otherwise known as P1 centres), which are paramagnetic defects.

Findings from Prooth *et al.* do not match original predictions, as the CVD approach was supposed to mitigate such defects. This discrepancy can be explained by comparing the fabrication techniques of Prooth *et al.* and Trusheim *et al.*. The paper by Trusheim *et al.* reported a sharp increase in coherence times, reaching up to 210 μs [34]. This paper followed a top-down fabrication process where reactive ion etching was used on a high-purity CVD-grown diamond to produce NDs. The significant improvements in coherence times were attributed to the low nitrogen content, which reduced the number of paramagnetic defects and allowed for greater average spacing between NV-centres.

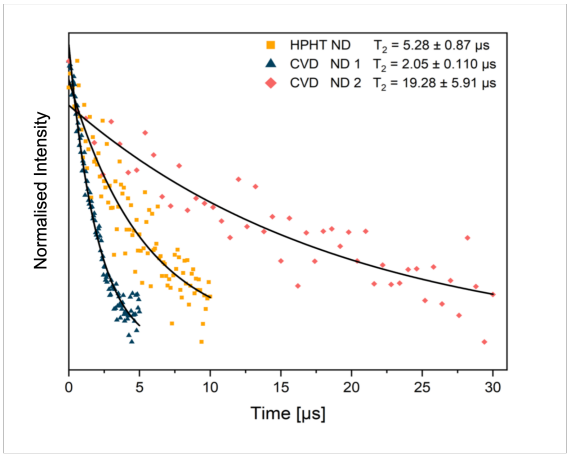

Figure 5: *Coherence lifetime of two CVD-grown NDs and one HPHT-grown ND. The pulse sequence used in this study was a Hahn Echo sequence for all NDs. Figure adapted from Prooth et al. in the supplementary information. [29].*

As mentioned, Prooth *et al.* follows a bottom-up fabrication approach where the shell-doped NDs had very high nitrogen concentrations, which may have contributed to P1 centres, thus leading to less improved coherence times [29]. However, in the supplementary information, the second group of CVD-grown NDs ($T_2^{(Hahn\ Echo)}$ = 19.28 $\pm$ 5.91 μs) outperforms the HPHT NDs ($T_2^{(Hahn\ Echo)}$ = 5.28 $\pm$ 0.87 μs) (Figure 5). Still, it does not exhibit the sudden increases seen in Trusheim *et al.*. Through comparative analysis, Prooth *et al.* may not have seen significant improvement due to the high nitrogen concentrations used for the shell doping situation. This facilitates the paramagnetic defects, specifically, P1 centres, to form, and causes the formation of NV-centres at closer proximity to one another, diminishing their spin-coherence characteristics.

4.2 Suppressing Presence of Dangling Bonds

As mentioned, magnetic noise and electric noise may lead to spin decoherence; however, electric noise may sometimes even dominate over magnetic noise [28]. Unsatisfied carbon bonds, otherwise known as dangling bonds, may be located on the surface of NDs and can generate

electric noise, thus diminishing the NV-centres spin-coherence times [31]. In addition, dangling bonds can cause NDs to be chemically unstable, thus compromising their biocompatibility [35]. Surface termination is a processing step used to enhance the outermost layer of NDs, which may satisfy unpaired carbon bonds [36]. This review focuses specifically on hydrogen and oxygen surface termination. Other methods, such as fluorine termination, are also studied, but these alternatives may disrupt the biocompatibility of NDs [37]. In addition, this review will explore a recent etching technique used to reduce the presence of dangling bonds.

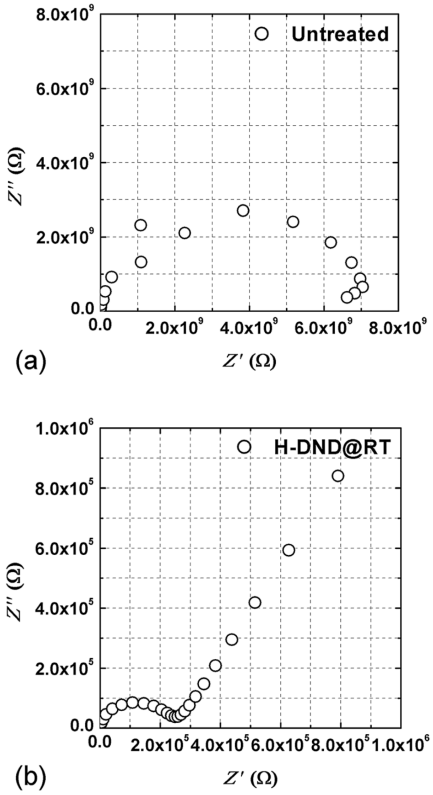

Figure 6: *Plots of the imaginary component of impedance against the real component of impedance for NDs using impedance spectroscopy. (a) Detonated NDs with no hydrogen treatment. (b) Detonated NDs that have hydrogen termination at room temperature. Figure adapted from Su et al. [38].*

Hydrogen termination (HT) is a type of surface termination technique where hydrogen atoms (H) saturate dangling bonds present on the surface of NDs. Su *et al.* investigated the difference in conductivity between untreated NDs and the HT-NDs, both of which had shallow NV-centres [38]. This was done by using commercially available detonated nanodiamond powders (SIGMA-Aldrich Corp.) that were H-terminated via microwave plasma-enhanced CVD. These powders were sandwiched between two copper plates, one of which was polished and had been electroplated by using high-purity nickel. Using this setup, impedance spectroscopy (IS) was conducted, which measured the electric and dielectric properties of the H-terminated powder. IS measurements involve finding the real and imaginary impedance of a sample, which can be expressed in the following equation:

$$Z(\omega) = Z' + jZ''. \tag{4}$$

$Z(\omega)$ is total impedance as a function of angular frequency ω. In addition, Z' represents the component of the real impedance and Z'' represents the component of the imaginary impedance. The findings show that NDs that are untreated exhibited a resistance four magnitudes greater (Figure 6(a)) in comparison to the hydrogen-terminated NDs. The improved conductivity of the NDs after HT indicates a significant reduction of dangling bonds, as they can trap charge carriers, thus preventing smooth conduction [20]. Therefore, the lack of dangling bonds suggests fewer charge fluctuations, which reduces electric noise that may cause spin decoherence.

While HT may improve the conductive properties of NDs, it was reported by Hauf *et al.* that HT benefits the formation of NV^0 centres (as opposed to the desired NV^- centres), this is because HT contributes to a negative electron affinity [39]. Additionally, excessive conduction of the NDs can lead to side effects such as unwanted interactions with biological surroundings due to heat generation on the surface. Oxygen-termination (OT) is another method where oxygen atoms (O) are employed and is found to assist the formation NV^- centres,

due to OT promoting positive electron affinity as per Hauf *et al.* [39]. Additionally, it favours a hydrophilic surface, ensuring better interactions within biological fluids, whereas HT tends to render the surface hydrophobic [36]. However, NDs that undergo OT do not passivate dangling bonds as effectively as NDs that undergo HT [15]. HT passivates dangling bonds by forming C-H bonds, which fully satisfy the valency of carbon and render the surface chemically inert. In the case of OT, various functional groups forming, such as $=$O, $-$C$-$O$-$C, can be due to oxygen's high chemical reactivity. Thus, oxygen introduces a mixture of surface states which affect the chemical stability of NDs and prevent complete passivation of dangling bonds. To address the issues that hydrogen and oxygen termination have, a combination of both methods allows for tunable and desirable characteristics [40].

The recent paper by Sun *et al.* was able to simulate the deposition of O and H atoms at a ratio of 2:1 and was able to saturate all dangling bonds as it had a surface coverage of greater than or equal to 1 [40]. In addition, the paper finds that a combination of HT, OT, and hydroxyl-termination promotes a positive electron affinity in NDs, which favours NV^- centres. Furthermore, this specific combination of different terminations was found to prevent unwanted surface states from forming and minimize spin noise, thus maintaining the NV-centre stability. The effects on spin-coherence were not reported, however, the reduction in spin noise and dangling bonds would suggest significant coherence time performance.

Previously, synthesis techniques for NDs, such as CVD [29], were discussed. Another common method to synthesis nanodiamonds is through ball milling, which involves using rotations/vibrations of hard balls to crush the sample into NDs [8]. A result of this is the presence of dangling bonds due to intense collision and grinding. Where surface treatments such near-field etching [41] can be employed for surface modification.

Research conducted by Brandenburg *et al.* showed a 25% increase in spin-coherence times when using near-field etching on NDs of approximately 200 nm with single NV-centres, compared to non-etched NDs [41]. Specifically, a helium-cadmium (He-Cd) laser with a wavelength of 325 nm was used to irradiate NDs, which were dispersed on a silicon substrate, with oxygen molecules as an etching source. During this procedure, the size of the NDs were changed, and so were their surface properties. The findings show that NDs that have an etching time of up to 60 minutes, showcased an increase in coherence time from initially $T_2^{(Hahn\ Echo)} \approx 1600$ ns up to $T_2^{(Hahn\ Echo)} \approx 2000$ ns (Figure 7). A significant increase of 25%, however, the coherence time was seen to drop after an hour, where the coherence time dropped to almost 1200 ns after 225 minutes of etching.

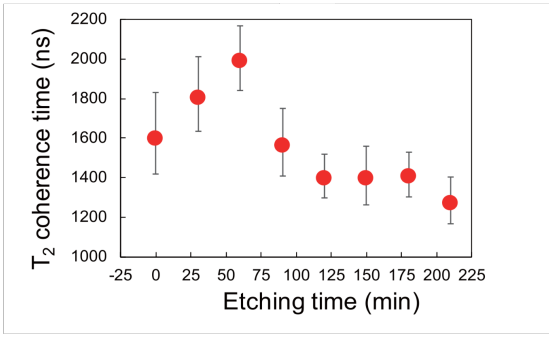

Figure 7: *Coherence time against near-field etching time for single NV-centre nanodiamonds. The pulse sequence used for this experiment was the Hahn-Echo sequence. Figure adapted from Brandenburg et al. [41].*

Brandenburg *et al.* determined that during the first hour, the presence of dangling bonds and unwanted terminated groups was expelled [41]. However, over-etching was seen to create newly emerging dangling bonds and oxygen molecules being adsorbed on the surface of the NDs.

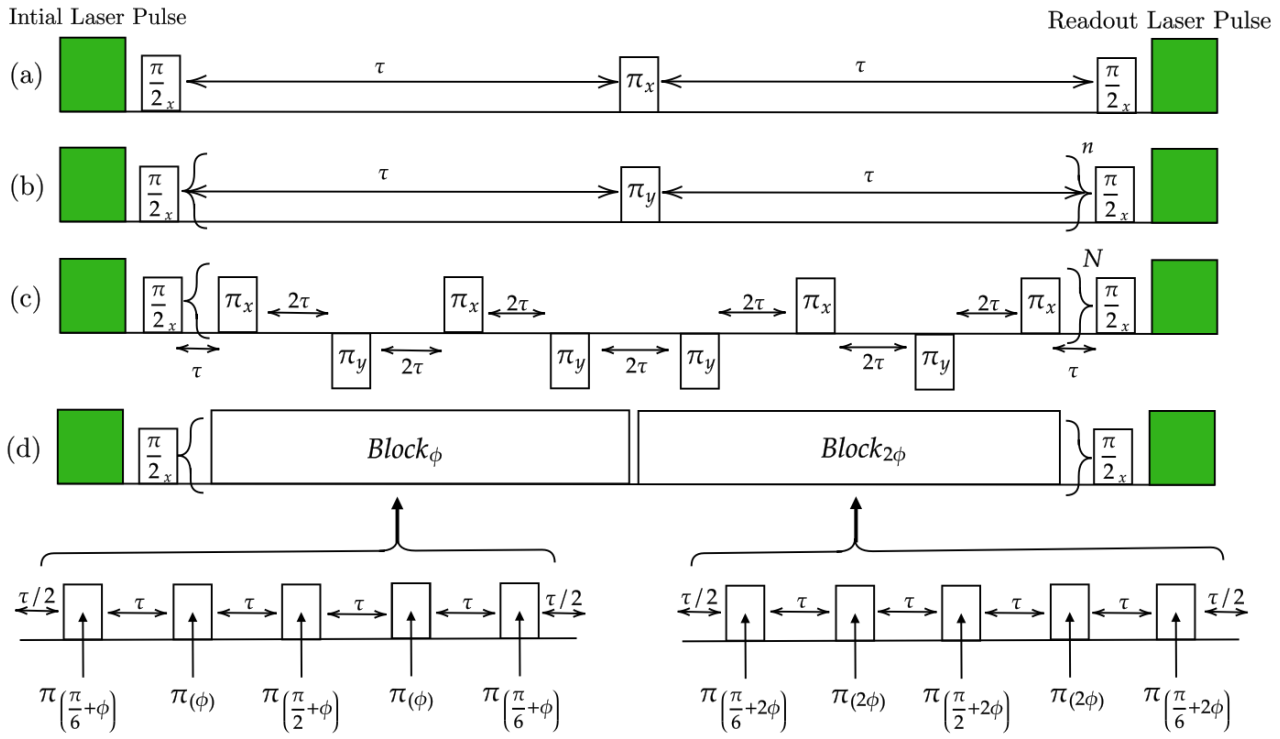

Figure 8: *Microwave pulse sequences investigated to make a comparative analysis, where τ represents the free evolution time between adjacent pulses. (a) The Hahn-Echo sequence uses an individual π pulse in the x direction. (b) The Carr-Purcell-Meiboom-Gill (CPMG) sequence is a π pulse in the y direction and can be repeated n times. (c) The XY8-N sequence uses periodic π pulses in the x,y direction and is repeated N times. (d) The Knill Dynamical Decoupling sequence is a composite pulse sequence in blocks which follow different phase shifts. Figures were inspired from [42] and [17].*

5 Pulse Sequences

In this review paper, different synthesis and treatment protocols have been discussed to improve the spin-coherence times of NDs. Another method which can be employed is altering the microwave pulse sequence used, however, NV-centres located near the surface of NDs have a randomly orientated axis. Thus, performing ODMR measurements is difficult [1]. Additionally, the standard Ramsey sequence ($\frac{\pi}{2} - \frac{\pi}{2}$ MW-pulses) suffers from T_2^* dephasing effects [17], thus returns the T_2^* dephasing time. Furthermore, biological systems are inherently noisy as factors such as thermal noise, biological magnetic noise, and motion-induced noise affect the coherence times of the NV-centres [9], [10]. Hence, more advanced pulse sequences are employed to combat both issues above and enhance the coherence times. This section discusses the Hahn-Echo (HE) sequence, the Carr-Purcell-Meiboom-Gill (CPMG) sequence, the XY8-4 sequence, and the Knill Dynamical Decoupling (KDD) sequence.

Erwin Hahn demonstrated the Hahn-Echo pulse sequence (Figure 8(a)) to combat spin-dephasing effects by the use of a π MW-pulse, which inverts electron spins and causes phase noises in the first and second τ to cancel one another along a single axis [42]. This extends the spin-coherence by using these refocusing pulses. In 2023, March *et al.* synthesised ball-milled NDs of 100 nm in diameter with single NV-centres. Five batches of NDs were produced, and the Ramsey sequence gave a mean value

of T_2^* = 1.35 ± 0.20 μs [17]. When using the HE-sequence, a value $T_2^{(HE)}$ = 25.8 ± 5.2 μs was measured. These findings are consistent with older studies such as work by Liu *et al.* in 2014, who used commercially available NDs ranging from 10 to 100 nm [43]. The Ramsey sequence reported a value of T_2^* = 0.703 μs and the HE-sequence reported $T_2^{(HE)}$ = 5.100 μs. The HE-sequence effectively mitigates dephasing, as shown by increased spin-coherence lifetimes in both studies. However, the HE-sequence is vulnerable to dynamic fluctuations in the environment, such as those seen in biological environments, where it is constantly changing [10].

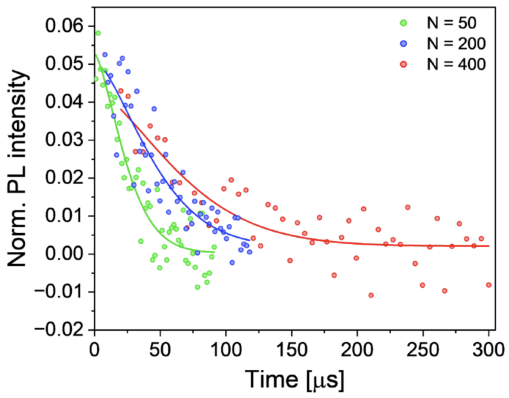

Figure 9: *Evolution of the CPMG sequence as the number of pulses increases. At 50 pulses,* $T_2^{(CPMG)}$ *= 28.3 μs. With 200 pulses,* $T_2^{(CPMG)}$ *= 52.8 μs, and at 400 pulses,* $T_2^{(CPMG)}$ *= 77.5 μs. Figure adapted from Oshimi et al. [44].*

The CPMG-sequence (Figure 8(b)) was named after Carr, Purcell, Meiboom, and Gill, who invented it as an extension of the HE-sequence [45]. This method is more resilient to environmental noise due to the inclusion of multiple π-MW pulses along the y-axis, thus enhancing spin-coherence. In 2024, Oshimi *et al.* showcased NDs synthesised via a top-down approach where single-crystalline bulk diamonds produced via HPHT were ground to sizes of around 80 nm [44]. The measurements from the CPMG-sequence at n = 50, resulted in spin-lifetime of $T_2^{(CPMG)}$ = 28.3 μs, whereas when the HE-sequence was used, the measurement reported $T_2^{(HE)}$ = 1.7 μs. Additionally, the CPMG-sequence coherence times depended on how many cycles the CPMG-sequence went through (Figure 9). Where at n = 400, the coherence times increased up to $T_2^{(CPMG)}$ = 77.5 μs.

Results from Oshimi *et al.* align with previous studies, such as that of Andrich *et al.* in 2014 [44], [46]. This paper reported values of $T_2^{(HE)}$ = 360 μs and $T_2^{(CPMG)}$ = 710 μs, though the *n* value was not specified. Andrich *et al.* used diamonds grown via plasma-enhanced CVD, with electron beam lithography later creating cylindrical NDs [46]. Both findings confirm the superiority of the CPMG sequence over the HE sequence, which is consistent with theoretical reasoning. This suggests that the CPMG sequence is particularly effective in maintaining long coherence, which is crucial in biological environments where noise is continuously and variably present.

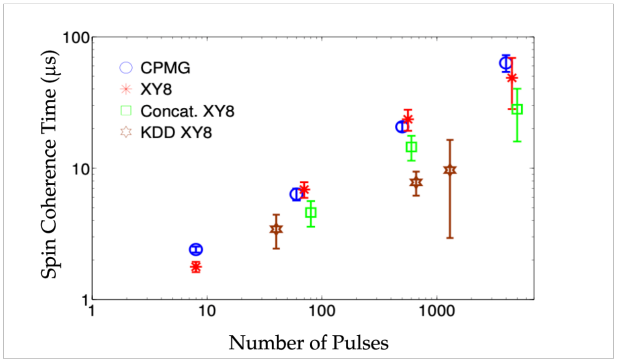

Figure 10: *Experimental results of various pulse sequences. Namely, the sequences compare the CPMG, XY8-N, the Concat. XY8-N sequence (a sequence with multiple layers of the XY8-N sequence), and the KDD-sequence. Figure adapted from Farfurnik et al. [47].*

While the CPMG-sequence extends the spin-coherence despite being in noisy environments, it is affected by imperfections in the control pulse (pulse errors). The XY8-N sequence (Figure 8(c)), reported by Gullion *et al.*, was developed

to address this and is described to extend the CPMG-sequence [45]. This sequence includes periodic π-MW pulses on the x and y axes, minimising pulse errors. Recent comparative studies of the CPMG and XY8-N pulse sequences have been focused on bulk diamonds since 2015 [47]. These studies focus on shallow NV-centres in bulk diamonds, effectively illustrating how NDs with near-surface NV-centres might perform. However, bulk diamonds with deep NV-centres would not provide the most accurate representation, as environmental noise is significantly reduced. Thus, deep NV-centres in bulk diamonds would have significantly better spin-coherence properties in comparison to NDs.

The findings of Farfurnik *et al.* conducted work on bulk diamonds with shallow NV-centres present intriguing findings about pulse sequences [47]. They find the coherence times of CPMG and XYn-N sequence progress similarly with increasing n and N values (Figure 10). The XYn-N sequence was originally expected to outperform the CPMG-sequence; this discrepancy can be explained by the low temperature setting at 77 K, which decreases electron-phonon interactions [48]. Electron-phonon interactions are another source of noise which may cause pulse errors that the XYn-N sequence can mitigate, but the CPMG-sequence may not [48], [23]. The decrease in electron-phonon interactions may result in fewer experienced pulse errors, negating the advantages the XY8-sequence typically holds over the CPMG-sequence. Consequently, the CPMG-sequence performs equally well with the XY8-sequence in these conditions. This may be further supported by the findings of Wang *et al.* which compared the CPMG-sequence and XY8-N sequence at room temperature.

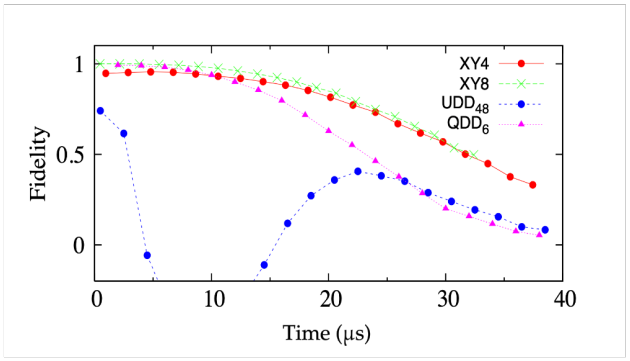

(a)

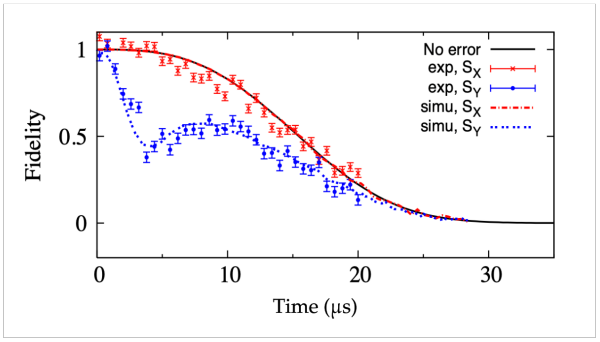

(b)

Figure 11: *Investigation of fidelity (a measure of the degree of similarity between the expected spin state and the actual outcome, where 1 is identical states and 0 completely different [49]) as a function of total evolution time for different pulse sequences. (a) Analysis of different sequences where the XY family dominates, UDD refers to the Uhrig Dynamic Decoupling sequence, and QDD refers to the Quadratic Dynamic Decoupling sequence. (b) Fidelity of the CPMG-sequence, where the simulation (dotted line plot) and experimental results (individually plotted points) are plotted for spin states in the x and y direction, S_X (red colour) and S_Y (blue colour) respectively. Figure adapted from Wang et al. [50].*

In 2012, Wang *et al.* studied bulk diamonds at room temperature. Their findings provide valuable insights comparing the CPMG and XY8-N sequences [50]. Wang *et al.* finds that the decoupling fidelity (a measure of the degree of similarity between the expected spin state and the actual outcome [49]) of the CPMG-sequence decays faster than the XY8-N sequence, drop-

ping to a fidelity value of 0 between 25 to 30 μs (Figure 11(a)) [50]. In contrast, the XY8-N sequence extends past 35 μs at N = 6 (Figure 11(b)). The XY8-N sequence excels by effectively suppressing accumulated pulse errors at room temperature. However, formal literature supporting the claim of the XY8-N sequence mitigating electron-phonon interactions could not be found, but it creates the need for further research to understand these sequences more. Studies comparing the XY8-N and the CPMG sequence have been outdated, possibly due to the rise of more complex pulse sequences, such as composite pulse sequences, which will be discussed.

Composite pulse sequences offer an alternative approach to previously mentioned sequences and are primarily attractive for their ability to reduce off-resonance errors [42]. These sequences deliver MW pulses at carefully chosen phase angles (ϕ) representing the angle between the x and y axes. An example of such a sequence is the KDD-sequence, a method primarily targeted at quantum computing and quantum memory as per Souza *et al.*. Literature using this sequence on NDs could not be found, however, the potential and its characteristics are fascinating [51]. It consists of a cyclic series of composite π-pulses with a phase shift of $\phi = \pm\frac{\pi}{3}$ [51] (Figure 8(d)), which is often described to be one of the more complex sequences.

Simulation work in a separate paper by Souza *et al.* (Figure 12) shows the performance of the CPMG-sequence, XY-4 (N=8) sequence, and the KDD-sequence [51]. To conclude each sequence performance, the number of oscillations that occur for each sequence when changing the flip angle error ($\Delta\theta$) can be studied. The CPMG-sequence is the most susceptible as its fidelity is seen to dramatically change when even under small amounts of $\Delta\theta$. It was found that the CPMG-sequence fidelity drops below 95% at $\Delta\theta \approx 2\%$. The XY8-4 sequence performs better than the CPMG-sequence, where the

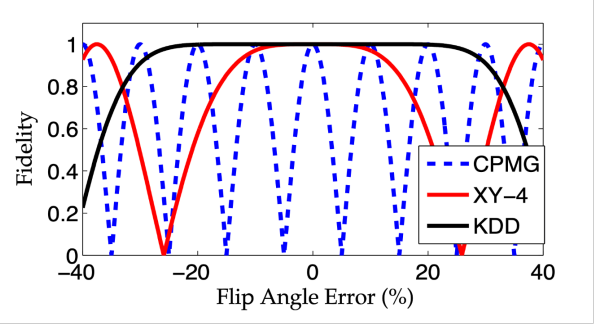

Figure 12: *Simulation results comparing the fidelity as a function of flip angle error (the angle difference between the intended angle and actual angle for a given spin state) for the CPMG, XY-4, and KDD-sequences. Figure obtained from Souza et al. [51].*

distance between crests is greater, implying the XY8-N sequence is more resilient to flip angle errors. This is further shown by its fidelity dropping below 95% at $\Delta\theta \approx 10\%$. However, the performance of the KDD sequence outperforms them both, where its fidelity drops below 95% with $\Delta\theta \approx 30\%$. The flip angle error is an important error consideration, as the stochastic environment of biological media can cause the angles of intended spin states to deviate by very noticeable amounts.

Returning to the paper by Farfurnik *et al.*, the KDD-sequence in Figure 10 is seen to reduce over the increasing number of pulses [47]. The KDD-sequence, while robust against flip angle errors, was susceptible to phase errors due to its phase differences between immediate pulses going as low as $\frac{\pi}{3}$. Thus, causing a decrease in coherence time. This can be mitigated through pulse calibration techniques, however, tailored methods for the KDD-sequence need to be further studied. Overall, the KDD-sequence shows potential use in quantum sensing due to its resilience against flip angle errors, along with off-resonance errors as well; however, phase errors reduce the spin-coherence but can be resolved through methods such as pulse calibration.

6 Summary

This review article aimed to investigate the various methods to improve the coherence times of NDs for free radical detection. Currently, researchers who use NDs with near-surface NV-centres for quantum sensing in medicine take advantage of NV-centres relaxation times. This is because the NV-centres relaxation time does not decay as rapidly as their spin-coherence times. A major source of decoherence properties arises from poor surface characteristics in NDs, namely due to the presence of paramagnetic defects and dangling bonds. Additionally, the coherence times depend on the type of pulse sequence delivered, and thus, various sequencing methods were investigated.

In terms of reducing the presence of paramagnetic defects on the surface of NDs, the synthesis technique using CVD seems to be the most promising method with the least amount of paramagnetic effects compared to detonation and HPHT techniques [34], [31]. This is true for low nitrogen concentrations as a comparative analysis between Prooth *et al.* showcased high P1 centre formations when using high nitrogen contents, which did not cause a sharp rise in spin-coherence time [29] as compared with studies by Trushiem *et al.* [34].

In addition to reducing the presence of paramagnetic defects, processing steps aimed at removing dangling bonds were investigated. While literature may discuss other techniques, such as fluorine termination, these methods may not preserve the biocompatibility characteristics that hydrogen and oxygen termination aid with [37]. Simulation results showed that a combination of hydrogen and oxygen termination can successfully saturate dangling bonds present on the surface of NDs [40]. It is recommended to use a combination of the two methods as OT does not passivate dangling bonds as well as HT, however, OT does favour the formation of the desired NV^- centres, whereas HT favours the formation of NV^0 centres. Simulation results also find surface termination techniques involve a combination of H-, O-, and hydroxyl termination, which was found to favour NV^- centres and minimise surface states and spin noise [40]. In addition, literature by Brandenburg *et al.* was studied for using near-field etching to treat NDs. Studies showed a 25% increase in the spin coherence time at 60 minutes. However, the spin-coherence time decreased after 60 minutes due to newly emerging dangling bonds as a result of over-etching.

Through comparative analysis of the aforementioned pulse sequence, the CPMG-sequence may be the most suitable pulse sequence due to its extensive studies, and outperforms the HE-sequence (an already well-established pulse sequence). Recent studies in 2024 from Oshimi *et al.* show that HE-sequence reports $T_2^{(HE)} = 1.7$ μs, the CPMG-sequence reports $T_2^{(CPMG)} = 77.5$ μs at n = 400, proving the CPMG-sequence's dominance [44]. While the XY8-N sequence is often referred to as an extension of the CPMG-sequence, literature findings by Farfurnik *et al.* show the CPMG-sequence performing on par with the XY8-N sequence [47]. This discrepancy may be explained by the lack of electron-phonon interactions, as this study was conducted at a temperature of 77 K. The XY8-N sequence is may have been able to mitigate such effects as, works by Wang *et al.* at room temperature suggest that the XY8-N sequence may outperform the CPMG-sequence as its fidelity was held longer (passing 35 μs) in comparison to the CPMG-sequence, which drops to a value of 0 between 25-30 μs. However, additional studies must be conducted to confirm this hypothesis.

Literature findings conducting a comparative analysis between the CPMG-sequence and the XY8-N sequence may have been outdated due to more advanced pulse sequences. Namely, composite sequences, such as the KDD-sequence. This sequence was developed for quantum computing and memory; literature findings in the context of NDs could not be

found. However, the simulation findings by Souza *et al.* showed that the KDD sequence mitigated flip angle errors significantly noticeably better than the CPMG and the XY8-N sequence, in addition to being able to reduce off-resonance errors as well. However, findings from Farfurnik *et al.* showed the KDD-sequence was susceptible to phase errors, and phase correction techniques must be investigated for this sequence [47].

7 Outlook

This review paper delved into different methods of synthesis techniques, surface treatment methods, and pulse sequences to enhance the coherence times of NDs with near-surface NV-centres. I believe a combination of these methods may allow for the spin-coherence time to be a parameter used to investigate the presence of free radicals. Examples may include using a combination of CVD-grown NDs with low nitrogen concentrations that are O- and H-terminated with a CPMG-sequence. Other examples may include researching with more emerging pulse sequences, such as the composite pulse sequence; the KDD-sequence.

However, there is room for more improvement in optimising the spin-coherence time. Prooth *et al.* used a top-down approach to grow NDs based on CVD, whereas Trusheim *et al.* employed a bottom-up approach to produce NDs through CVD [29], [34]. I believe it is worth exploring which method, between the top-down and bottom-up approach, ensures better shape and control of when growing NDs through CVD. Better shape and control reduce overall surface roughness and reduce the occurrence of trapped charges, for example. Additionally, the effects that some techniques may have on other techniques must be studied beforehand. Namely, the effects that near-field etching will have on NDs that have either been O- and H-terminated or O-, H-, and hydroxyl-terminated. In addition, research investigating the use of composite sequences such as the KDD-sequence in the context of NDs is a question to be addressed, and its performance compared to sequences such as the CPMG and XY8-N sequence.

From my analysis, results in optimising the surface characteristics of NDs have been improving over time, where improvements in various synthesis techniques and processing methods have been made [1], [8], [26]. An ongoing issue that needs to be addressed is the reusability of NDs after their use in biological environments, as they are often disposed of after one use [9]. This is not only expensive long term but also unsustainable. To address this issue, research into different kinds of cleaning methods must be conducted. This is important when considering NDs with enhanced coherence properties, as fabricating these NDs is more expensive; thus, having reusable NDs is a factor to consider.

Overall, the current ongoing research in pulse sequences for NV-centres is primarily focused on bulk diamonds for quantum computing and quantum memory applications. However, the progress of quantum sensing in medicine has been on the rise; for example, in 2025, a UMCG spin-off company named QTSense[2] received a sum of €6 million[3] to advance studies indicating the potential of quantum sensors. I believe over the coming years, more research output on NDs and specifically, using them in medicine, will be on the rise.

The intertwining between nanoscience and medicine has been steadily rising in recent years. The presence of quantum dots is currently in clinical trials for tumour imaging [52], in nanomedicine, where lipid nanoparticles were used as mRNA carriers for the COVID-19 vaccinations by Pfizer-BioNTech [53]. The use of quantum sensors has impacted the medical

[2] https://www.qtsense.com

[3] https://www.eu-startups.com/2025/02/qt-sense-raises-e6-million-to-understand-diseases-at-a-single-cell-level-with-quantum-sensing/

field. An article [4] at the RUG was published last year discussing an early sepsis diagnosis linked with free radicals. I believe the amount of potential and funding going into the use of quantum sensors within medicine is increasing, and issues, as previously mentioned, can be mitigated to bring nanoscience much closer to patient care.

8 Personal Note

On a personal note, as I am working within the Department of Surgery and the Department of Nuclear Medicine and Molecular Imaging at the UMCG, I am usually in close contact with medical doctors/physicians or soon-to-be medical doctors. Their excitement when I tell them about NDs with near-surface NV-centres is astonishing. Some have talked about how they could be incorporated into studying oxidative stress within the Department of Experimental Cardiology. Others have talked about how it could be used to monitor free radicals of patients in the surgical theatre during organ transplants. The opportunities these quantum sensors have are immense.

9 Acknowledgements

I would like to thank Prof. Dr. Ir. Caspar van der Wal for firstly, being an overall amazing, supportive, and present supervisor. I would like to thank those weekly meetings from February up until April. These meetings were extremely insightful, and I have learnt a lot from him. This review paper has been difficult, in terms of content, and as a task for me, and having a supervisor like Prof. Dr. Ir. Caspar van der Wal played a major role in making this journey less daunting. It has been a privilege working with him, and I thank him once again.

I would like to thank Prof. Dr. Romana Schirhagl for an online meeting during my review paper time, who provided me with clarity on doubts I had when writing this paper.

I acknowledge the use of Grammarly by Grammarly, Inc., which provided **improvements** to my grammar and punctuation in the **already written text**.

[4] https://www.rug.nl/fse/news/health-and-life/20241205-freeradicalsforearlydiagnosisofsepsis?lang=en

References

1. Aslam, N. *et al.* Quantum sensors for biomedical applications. *Nature Reviews Physics* **5,** 157–169 (2023).
2. Formica, D. & Schena, E. Smart Sensors for Healthcare and Medical Applications. *Sensors* **21,** 543 (2021).
3. Sutton, P. A. *et al.* Fluorescence-guided surgery: comprehensive review. *BJS Open* **7,** zrad049 (2023).
4. Heeman, W. *et al.* A guideline for clinicians performing clinical studies with fluorescence imaging. *Journal of Nuclear Medicine,* jnumed.121.262975 (2022).
5. Keizers, B. *et al.* Systematic comparison of fluorescence imaging in the near-infrared and shortwave-infrared spectral range using clinical tumor samples containing cetuximab-IRDye800CW. *Journal of Biomedical Optics* **30** (S1 2024).
6. Oh, E. & Gregoire, M. D. A Perspective on Quantum Sensors from Basic Research to Commercial Applications.
7. Fox, M. *Optical properties of solids* 2. ed., reprinted. *Oxford master series in condensed matter physics* **3.** 396 pp. ISBN: 978-0-19-957336-3 (Oxford Univ. Press, Oxford, 2012).
8. Qin, J.-X. *et al.* Nanodiamonds: Synthesis, properties, and applications in nanomedicine. *Materials & Design* **210,** 110091 (2021).
9. Mzyk, A., Sigaeva, A. & Schirhagl, R. Relaxometry with Nitrogen Vacancy (NV) Centers in Diamond. *Accounts of Chemical Research* **55,** 3572–3580 (2022).

10. Li, R. *Diamond-based Sensors and Biolabels for Biomedical Applications:* PhD thesis (University of Groningen, 2023).

11. Budakian, R. *et al.* Roadmap on nanoscale magnetic resonance imaging. *Nanotechnology* **35,** 412001 (2024).

12. Reyes-San-Martin, C. *et al.* Diamond-based quantum sensing of free radicals in migrating human breast cancer cells. *Carbon* **228,** 119405 (2024).

13. La Via, L. *et al.* The Global Burden of Sepsis and Septic Shock. *Epidemiologia* **5,** 456–478 (2024).

14. Bushberg, J. T., Seibert, J. A., Leidholdt, E. M. J. & Boone, J. M. *The essential physics of medical imaging* 3rd edition. In collab. with Ovid Technologies, Inc. 1 p. ISBN: 978-0-7817-8057-5 978-1-4698-2155-9 (Wolters Kluwer Health/Lippincott Williams & Wilkins, Philadelphia, 2012).

15. Schirhagl, R., Chang, K., Loretz, M. & Degen, C. L. Nitrogen-Vacancy Centers in Diamond: Nanoscale Sensors for Physics and Biology. *Annual Review of Physical Chemistry* **65,** 83–105 (2014).

16. Gould, K. in *Encyclopedia of Applied Plant Sciences* 9–16 (Elsevier, 2003). ISBN: 978-0-12-227050-5.

17. March, J. E. *et al.* Long spin coherence and relaxation times in nanodiamonds milled from polycrystalline 12 C diamond. *Physical Review Applied* **20,** 044045 (2023).

18. Shinei, C. *et al.* Nitrogen related paramagnetic defects: Decoherence source of ensemble of NV-center. *Journal of Applied Physics* **132,** 214402 (2022).

19. Li, L.-s. & Zhao, X. Dangling bond-induced graphitization process on the (111) surface of diamond nanoparticles. *The Journal of Chemical Physics* **134,** 044711 (2011).

20. Rodgers, L. V. H. *et al.* Materials challenges for quantum technologies based on color centers in diamond. *MRS Bulletin* **46,** 623–633 (2021).

21. Pham, L. M. *et al.* Enhanced metrology using preferential orientation of nitrogen-vacancy centers in diamond. *Physical Review B* **86,** 121202 (2012).

22. *Breast MRI: Fundamentals and Technical Aspects* (ed Hendrick, R. E.) (Springer Science+Business Media, LLC, New York, NY, 2008). 254 pp. ISBN: 978-0-387-73506-1 978-0-387-73507-8.

23. Kittel, C. *Introduction to solid state physics* 8th ed. 680 pp. ISBN: 978-0-471-41526-8 (Wiley, Hoboken, NJ, 2005).

24. Bl, e., Stephen, B. & ell, K. M. Concepts in Thermal Physics.

25. Amin, R. S., Nikolaidis, P., Kawashima, A., Kramer, L. A. & Ernst, R. D. Normal Anatomy of the Fetus at MR Imaging. *RadioGraphics* **19,** S201–S214 (suppl_1 1999).

26. Chipaux, M. *et al.* Nanodiamonds and their applications in cells. *Small* **14,** 1704263 (2018).

27. Narayan, R. J., Boehm, R. D. & Sumant, A. V. Medical applications of diamond particles & surfaces. *Materials Today* **14,** 154–163 (2011).

28. Kim, M. *et al.* Decoherence of Near-Surface Nitrogen-Vacancy Centers Due to Electric Field Noise. *Physical Review Letters* **115,** 087602 (2015).

29. Prooth, J. *et al.* Long Spin Relaxation Times in CVD-Grown Nanodiamonds. *Advanced Quantum Technologies* **6,** 2300004 (2023).

30. Dolmatov, V. Y. Corrections to the article by V. Yu. Dolmatov 'Detonation synthesis nanodiamonds: synthesis, structure, properties and applications', *Russian Chemical Reviews* , **76** 339-360 (2007). *Russian Chemical Reviews* **77,** 303–303 (2008).

31. Nagl, A., Hemelaar, S. R. & Schirhagl, R. Improving surface and defect center chemistry of fluorescent nanodiamonds for imaging purposes—a review. *Analytical and Bioanalytical Chemistry* **407,** 7521–7536 (2015).

32. Boudou, J.-P. *et al.* Fluorescent nanodiamonds derived from HPHT with a size of less than 10nm. *Diamond and Related Materials* **37,** 80–86 (2013).

33. Song, X. *et al.* Generation of nitrogen-vacancy color center in nanodiamonds by high temperature annealing. *Applied Physics Letters* **102,** 133109 (2013).

34. Trusheim, M. E. *et al.* Scalable Fabrication of High Purity Diamond Nanocrystals with Long-Spin-Coherence Nitrogen Vacancy Centers. *Nano Letters* **14,** 32–36 (2014).

35. Krueger, A. in *Nanodiamonds* 183–242 (Elsevier, 2017). ISBN: 978-0-323-43029-6.

36. Jariwala, D. H., Patel, D. & Wairkar, S. Surface functionalization of nanodiamonds for biomedical applications. *Materials Science and Engineering: C* **113,** 110996 (2020).

37. Han, J. *et al.* Chemical Aspects of Human and Environmental Overload with Fluorine. *Chemical Reviews* **121,** 4678–4742 (2021).

38. Su, S., Li, J., Kundrát, V., Abbot, A. M. & Ye, H. Hydrogen-terminated detonation nanodiamond: Impedance spectroscopy and thermal stability studies. *Journal of Applied Physics* **113,** 023707 (2013).

39. Hauf, M. V. *et al.* Chemical control of the charge state of nitrogen-vacancy centers in diamond. *Physical Review B* **83,** 081304 (2011).

40. Sun, Z., Liang, P., Liu, Q., Cui, B. & Gao, N. Hydrogen and oxygen mixed-termination for nitrogen-vacancy quantum sensors in hexagonal diamond. *Vacuum* **219,** 112719 (2024).

41. Brandenburg, F. *et al.* Improving the electron spin properties of nitrogen-vacancy centres in nanodiamonds by near-field etching. *Scientific Reports* **8,** 15847 (2018).

42. Ho, K. O. *et al.* Diamond quantum sensors: from physics to applications on condensed matter research. *Functional Diamond* **1,** 160–173 (2021).

43. Liu, D.-Q., Liu, G.-Q., Chang, Y.-C. & Pan, X.-Y. Scaling of dynamical decoupling for a single electron spin in nanodiamonds at room temperature. *Physica B: Condensed Matter* **432,** 84–88 (2014).

44. Oshimi, K. *et al.* Bright Quantum-Grade Fluorescent Nanodiamonds. *ACS Nano* **18,** 35202–35213 (2024).

45. Jelezko, D. F. Amtierender Dekan: Prof. Dr. Peter Dürre.

46. Andrich, P. *et al.* Engineered Micro- and Nanoscale Diamonds as Mobile Probes for High-Resolution Sensing in Fluid. *Nano Letters* **14,** 4959–4964 (2014).

47. Farfurnik, D. *et al.* Optimizing a Dynamical Decoupling Protocol for Solid-State Electronic Spin Ensembles in Diamond. *Physical Review B* **92,** 060301 (2015).

48. Dhara, P. & Guha, S. Phonon-induced decoherence in color-center qubits. *Physical Review Research* **6,** 013055 (2024).

49. Liang, Y.-C. *et al.* Quantum fidelity measures for mixed states. *Reports on Progress in Physics* **82,** 076001 (2019).

50. Wang, Z.-H., Lange, G. d., Riste, D., Hanson, R. & Dobrovitski, V. V. Comparison of dynamical decoupling protocols for a nitrogen-vacancy center in diamond. *Physical Review B* **85,** 155204 (2012).

51. Souza, A. M., Álvarez, G. A. & Suter, D. Robust dynamical decoupling. *Philosophical Transactions of the Royal Society A: Mathematical, Physical and Engineering Sciences* **370,** 4748–4769 (2012).

52. Fang, M., Peng, C.-w., Pang, D.-W. & Li, Y. Quantum Dots for Cancer Research: Current Status, Remaining Issues, and Future Perspectives. **9** (2012).

53. Wilson, B. & Geetha, K. M. Lipid nanoparticles in the development of mRNA vaccines for COVID-19. *Journal of Drug Delivery Science and Technology* **74,** 103553 (2022).